Journal of Quantitative Spectroscopy & Radiative Transfer 263 (2021) 107557

Contents lists available at ScienceDirect

Journal of Quantitative Spectroscopy & Radiative Transfer

journal homepage: www.elsevier.com/locate/jqsrt

Line parameters for hot methane ν_3 band broadened by H_2 from 296 to 1100 K.

Mahdi Yousefi[a,a,*], Peter F Bernath[a,b], Mike Dulick[b], Manfred Birk[c], Georg Wagner[c]

[a] Department of Physics, Old Dominion University, Norfolk, VA 23529, USA
[b] Department of Chemistry & Biochemistry, Old Dominion University, Norfolk, VA 23529, USA
[c] Remote Sensing Technology Institute, German Aerospace Center (DLR), Weß ling, 82234, Germany

ARTICLE INFO

Article history:
Received 20 August 2020
Revised 1 February 2021
Accepted 1 February 2021
Available online 4 February 2021

Keywords:
High temperature methane
Fourier transform spectroscopy
Line parameters
Pressure broadening
Pressure shifts
Multi-spectrum fitting

ABSTRACT

Methane (CH_4) spectra in the ν_3 band near 3.3 m were measured for 0, 50, 150, 240, 320, and 400 Torr pressure of added hydrogen. The spectra were recorded using a high resolution Fourier transform spectrometer. The CH_4 spectra were measured at 5 different temperatures from room temperature up to ~ 1100 K. A multi-spectrum non-linear least squares fit method was used to determine the line parameters at each temperature. Voigt lineshape functions were used to determine the broadening and shifting of methane lines in the P and R branches. The temperature dependence of exponent parameters for the line width and the linear frequency shift coefficients were determined from a fit for temperatures ranging from 296 to 1098 K. The temperature dependence of the retrieved line broadening parameters was observed to follow the Double Power Law (DPL) proposed by Gamache and Vispoel. The temperature dependence of the pressure shift coefficients follows a linear trend for the first three temperatures. The pressure broadening parameters decrease with increasing temperature, and the pressure shift parameters increase with increasing temperature, especially for the first three temperatures. Finally, the dependence of pressure broadening (γ_0) and shift (δ_0) parameters on the rotational quantum number (J) was studied. The pressure broadening coefficients decrease about 20–30% for temperatures up to 894 K and about 40% for 1098 K, with increasing J quantum number. A complete set of fitted parameters including line position (σ), line intensity (S), pressure broadening (γ_0), shifting (δ_0), and their corresponding fitting errors are provided in supplementary tables.

1. Introduction

Recently, there has been great interest in methane-containing astronomical objects outside the Solar System, such as exoplanets including hot Jupiters [1–3], hot Neptunes [4–6] and super-Earths [7,8]. Methane has also been detected in the atmospheres of brown dwarfs, which are cool sub-stellar objects unable to fuse hydrogen in their cores [9]. Understanding the atmospheric composition of exoplanets and brown dwarfs gives valuable information on the history of planetary evolution [10], their appearance [2], the temperature profile [11], the chemical composition of the planet's core, the C/O ratio and so forth [9]. For example, an accurate measurement of CH_4 abundance can constrain the C/O ratio, which is an important factor in the chemical composition of the atmosphere as well as in classifying the exoplanet [2,5,12]. The atmospheres of these giant planets and brown dwarfs are complex and have opacities that vary strongly with wavelength [9].

Ground and space-based near-infrared spectroscopic observations have been essential for studying the atmospheres of exoplanets and brown dwarfs [1,11]. CH_4 is expected to be the main carbon-bearing molecule in the atmospheres of Jovian planets and brown dwarfs at temperatures up to about 1000 K [4,13].

Atmospheres of hot Jupiters and brown dwarfs are dominated by H_2. The main carbon-containing molecules are CO and CH_4, and their relative abundance depends on temperature and pressure [14]. In addition to observations, photochemical radiative transfer models are used to predict atmospheric composition [4,15]. These models require reliable opacities in order to correctly model the atmosphere [16]. Methane is the main contributor to the atmospheric opacity of hot Jupiters and brown dwarfs [1,17]. There have been many detections of H_2-dominated hot exoplanets (hot Jupiters) that contain significant amounts of CH_4.

To calculate atmospheric opacity of exoplanets and brown dwarfs, an accurate linelist for methane is required [18]. The avail-

* Corresponding author.
E-mail address: myous005@odu.edu (M. Yousefi).

https://doi.org/10.1016/j.jqsrt.2021.107557
0022-4073/

able exo-planetary models typically include thermal and pressure broadening of spectral lines in their opacity calculations. While thermal broadening of spectral lines is straightforward [19], the pressure broadening of spectral lines is more complicated and unique to each molecule [20,21]. In the case of H_2-dominated giant planets, the collisional interactions with H_2 result in broadened CH_4 lines [22–24]. It is useful to understand where the thermal and pressure broadening mechanisms are most significant in the pressure-temperature (P–T) space. A useful analysis was made by Hedges and Madhusudhan [25]. While thermal broadening increases with increasing temperature, for the pressure range of 50–400 Torr, used in this study, pressure broadening is the dominant mechanism; therefore, this study focuses on determining the pressure broadening coefficients for the methane spectra at elevated temperatures.

The line parameters needed include line position, strength, pressure-broadened line width and pressure-induced frequency shift as well as their temperature-dependence. Smith et al. measured the temperature-dependence of broadening and shifting of CH_4 spectral lines in the ν_4 band using air and N_2 at low temperatures and found a significant rotational dependence [28]. Varanasi and Chudmani also measured the temperature-dependence of broadening of methane in the ν_4 band at low temperatures [22].

In addition to measurements, there have also been theoretical studies predicting methane line parameters. Anderson used perturbation theory and related the pressure-induced broadening by a foreign agent to electrostatic intermolecular interactions [32]. Neshyba et al. [33] used complex Robert-Bonamy theory to describe line broadening and shifting in the CH_4-N_2 system. They found that repulsive intermolecular Lennard-Jones atom-atom interactions are the main contributor to linewidth broadening and that the broadening decreases with increasing J quantum number. Gabard [34] developed a semiclassical method for the broadening of methane lines perturbed by diatomic molecules using a symmetrized version of Robert-Bonamy theory. In addition, Smith and Secrest [35] developed a new interaction potential for the Ar-CH_4 collision system and calculated a total collision cross-section for different A, E and F rotational symmetry levels. They concluded that the total collisional cross-section for the E component is smaller than for the A and F components. This was in agreement with Smith et al.'s [28] conclusion about the symmetry dependence of line broadening from Fourier transform infrared measurements of the ν_4 mode.

The Voigt profile is the standard lineshape model used in high-resolution spectroscopy because of its relative simplicity. However, increasing sensitivity and accuracy of spectroscopic techniques enables the use of new lineshapes such as the Hartmann–Tran (H–T) lineshape model [36–38], also called the partially Correlated quadratic-Speed-Dependent Hard Collision Profile (pCqSD-HCP) model, in which additional effects such as speed-dependence of the broadening, shifting and collisional narrowing are taken into account. In this study, a Voigt profile is used to determine spectral line parameters such as pressure broadening and shifts. In addition to the Voigt profile, a quadratic speed-dependent hard collision (qSDHC) model in the Hartmann–Tran implementation [36,37] was also tried but did not improve the analysis and is not reported here.

The temperature-dependence of spectral lineshape parameters is often expressed as a single power law $\chi(T) = \chi(T_0) * (T_0/T)^n$, where T_0 is a reference temperature and $\chi(T_0)$ is the parameter at T_0. However, a single power law does not always explain the temperature-dependence of line parameters such as pressure broadening [28,37,38]. Gamache and Vispoel [39] developed a double power law expression that predicts the temperature-dependence of the broadening parameter over a large temperature range. Also, a linear temperature-dependence has been observed for the pressure-induced line shift [28,37,38].

While there have been extensive studies of methane line parameters, most studies have focused on the conditions for Earth's atmosphere at relatively low temperatures [26–31,40], only a few high temperature studies of the CH_4.H_2 system have been published for a limited range of temperatures and pressures [23,41]. In our study, we aimed to measure methane lineshape parameters as well as their temperature-dependence in the ν_3 band for both P and R branches in the presence of H_2. The goal is to measure methane pressure-induced line parameters for a large temperature range from room temperature to $\sim$ 1100 K. This study will contribute to a better understanding of hydrogen-dominated hot exoplanets and brown dwarfs.

2. Experimental set up

2.1. Instrumentation

All of the spectra were recorded using a Bruker 120/125 HR Fourier transform spectrometer (120 HR bench upgraded with 125 HR electronics) at the Old Dominion University at a spectral resolution of 0.01 cm^{-1} (MOPD = 90 cm). A schematic of the experimental arrangement is shown in Fig. 1. H_2 and CH_4 pressures were separately measured using two MKS Baratron pressure gauges (MKS 220 C model with 1000 Torr and MKS 626 B with 10 Torr maximum pressure) with $\sim$ 1% accuracy. The CH_4 and H_2 samples were stored in two separate tanks filled from gas cylinders at room temperature. The ideal gas law was used to calculate the amount of stored gas in the tanks that would achieve the desired pressure in the heated cell, at the temperature of the experiment. The cell was heated to the desired temperature with a CM Rapid Temp tube furnace. Then, CH_4 was added to the cell followed by H_2 from their storage tanks. The nominal temperature measurements were made using a thermocouple sensor provided by the furnace manufacturer. In a separate experiment, more accurate temperature measurements were carried out inside the furnace with another thermocouple at the nominal temperatures measured by the furnace thermocouple. The thermocouple was positioned inside the cell and parallel to its axis, to measure the temperature inhomogeneity. The inhomogeneity measurement was performed with air in the cell. Temperature measurements showed a maximum temperature at the center of the cell that drops by about 20 K at the ends of cell. Finally, all the analysis was performed using the temperatures measured by the thermocouple in the cell instead of the nominal temperatures measured by the thermocouple sensor on the furnace.

Because of the high temperature nature of the experiment, the 50.8 cm long cell was made of quartz (SiO_2) that has a high melting point. Light emitted from an infrared source (glowbar) was collimated with a lens outside the furnace, passed through the cell and was then focused onto the entrance aperture of the spectrometer with another lens. The spectral range of 1800–5500 cm^{-1} was selected using a Ge filter which removes the radiation above 5500 cm^{-1}, and an InSb detector. The InSb detector is very linear and was not saturated so no non-linearity correction was made.

2.2. Experimental conditions and recorded spectra

The goal of this study was to measure pressure-induced broadening and shifting coefficients of the ν_3 band of the methane lines at high temperatures. The CH_4 infrared spectrum was measured at five different calibrated temperatures of 296 K, 463 K, 681 K, 894 K, and 1098 K in the 2750–3200 cm^{-1} range. At each temperature, the CH_4 spectrum was measured at five different pressures of H_2 at 50, 150, 240, 320, and 400 Torr where the partial pressure

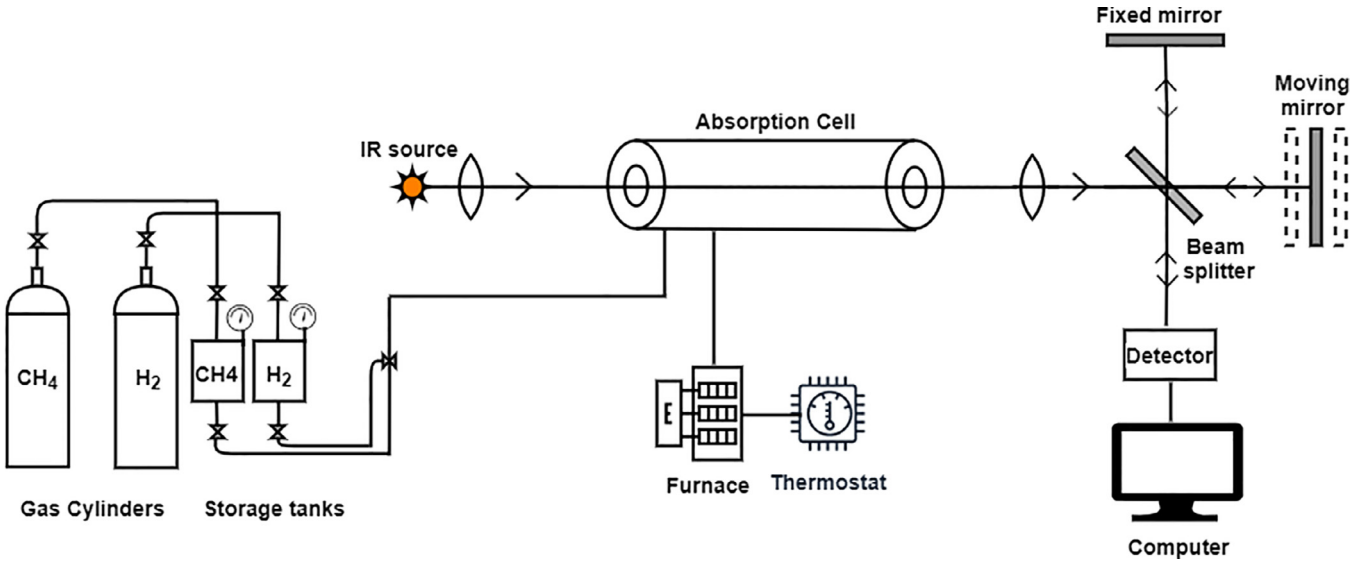

Fig. 1. Schematic view of the experimental setup including the gas cylinders, storage tanks, IR source, furnace, absorption cell and the Bruker 120/125 FTS.

Table 1
Experimental conditions for CH_4 spectra, with 0.5 Torr of CH_4 for all spectra and, five different H_2 pressures at each temperature.

Parameter	Value
Spectral region (cm^{-1})	1800–5400
Aperture diameter (mm)	2
Detectors	LN-InSb
Filter	Ge
Beamsplitter	CaF_2
Spectrometer windows	CaF_2
Lens	CaF_2
Cell pathlength (cm)	50.8
Scans	128
Resolution (cm^{-1})	0.01
H_2 pressures (Torr)	50, 150, 240, 320, 400
CH_4 pressure (Torr)	0.5
Temperatures (K)	296, 463, 681, 894, 1098

of CH_4 was 0.5 Torr for all the spectra. A summary of experimental conditions is provided in Table 1.

At the high temperature of the experiment, there is emission from the cell and from hot CH_4 in the recorded spectra. In this experiment, the true transmittance spectrum of CH_4 is required; therefore it is necessary to correct for emission. Four spectra were recorded: A, gas absorption (glowbar source with gas); B, gas emission (no glowbar with gas); C, cell emission (no source and no gas); and D, reference (glowbar source without gas). An example of four recorded spectra and the resulting gas transmittance is shown in Fig. 2. Each of the emission and absorption spectra were an average of 128 co-adds and the transmission spectrum is calculated as [45]

$$\tau = \frac{A - B}{D - C}. \quad (1)$$

The spectra (Fig. 2) showed some hot water impurity lines which were not included in our analysis. Methane lines that were overlapped by water lines were not analyzed.

3. Data analysis

3.1. Spectrum preparation: Line position calibration and continuum/baseline correction

All CH_4 spectra were converted from their interferograms using "boxcar" apodization with a zero filling factor of 2. The continuum baseline of the transmission spectra were not always at 100%. This is caused mainly by drifting of the infrared source over the period of data acquisition. The Bruker OPUS software was used for the continuum baseline correction. The transmission spectra were converted to absorbance and OPUS polynomial baseline correction was used to adjust the baseline value to zero. These baseline corrected absorbance spectra were converted back to transmission spectra.

The line positions were measured for each of the pure spectra for P and R branch lines; the Q branch lines were not measured because of severe blending. Then several isolated lines were selected and their positions were compared to HITRAN 2012 [42] values. For each temperature, a calibration factor was calculated by averaging the line position ratios for the selected lines. The calibration factors for the temperatures 296 K, 463 K, 681 K, 894 K, and 1098 K are 0.999996860(15), 0.999996917(28), 0.999996980(37), 0.999997302(18), 0.999997317(69), respectively, one standard deviation in the last two digits is quoted in parentheses. After calibration, the wavenumber scale is accurate to better than 0.0005 cm^{-1}. The precision of the line position measurement depends on the line width and the signal-to-noise ratio and is typically 0.0001 cm^{-1} as estimated for the 150 Torr spectrum at 463 K. A typical pressure shift for these condition is about -0.0015 cm^{-1}.

3.2. Line profiles and line parameter retrieval

A multi-spectrum non-linear least squares fit was performed to improve the determination of line parameters. Fitting was done with software developed at the German Space Agency (DLR) [37,38]. For each single temperature, a simultaneous non-linear least squares fit of all the parameters including line position (σ), line intensity (S), pressure broadening (γ_0) and shifting (δ_0) was carried out for spectra recorded at multiple pressures of H_2. The recorded spectra show broadened lines as a result of two mechanisms: Doppler broadening (resulting from the Maxwell-Boltzmann velocity distribution of absorbing particles) and collisional broad-

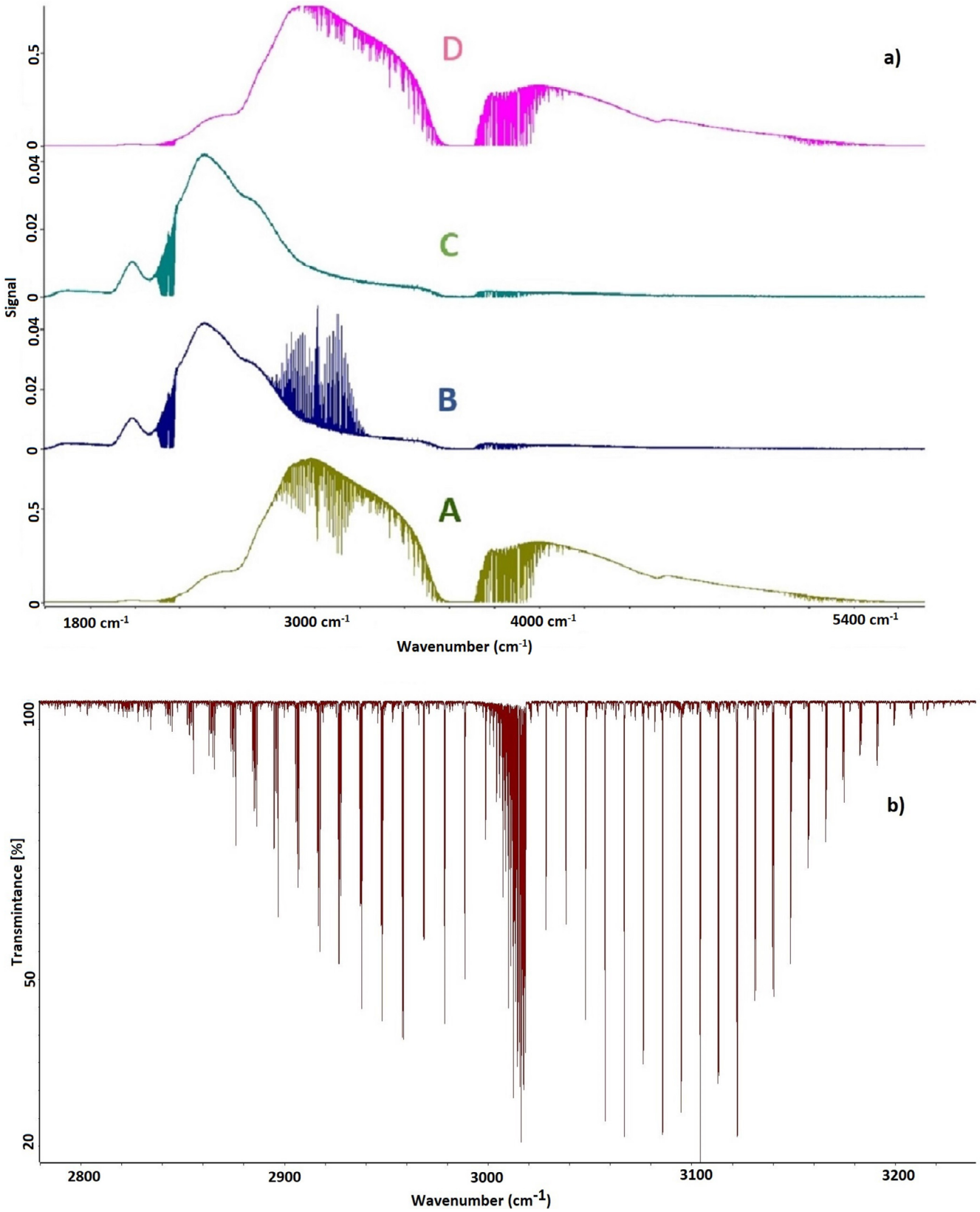

Fig. 2. (a) Four measured spectra with the 50.8 cm path length A. gas absorption B. gas emission C. cell emission D. glowbar reference (b) the resulting gas transmittance at 0.5 Torr CH_4, 150 Torr H_2 and 463 K in the ν_3 band of methane spectrum.

Table 2
Comparison between measured temperature and those obtained from a fit.

P (Torr)	T_{exp}(K)	T_{fit}(K)
50	296	294 (1.4)
50	463	460 (13)
50	681	681 (14)
50	894	878 (14)
50	1098	1098.8 (27)

ening (represented by a Lorentzian profile). A Maxwell-Boltzmann velocity distribution results in Doppler broadening, and collisional broadening is often represented by a Lorentzian profile. A Voigt profile is a convolution of Gaussian and Lorentzian profiles [43] and is frequently used for spectral fitting. The effect of the instrumental lineshape was included by using the sinc box function.

In this study, the Voigt lineshape was used to fit the CH_4 lines. Line position (cm^{-1}), line intensity (cm/molecule), pressure broadening (γ_0), and pressure shift (δ_0) parameters in units of cm^{-1}/atm were fitted simultaneously. Doppler broadening was set to a fixed value at the measured temperature.

3.3. Fit procedure

The multi-spectrum fitting program reproduces the measured spectra at each hydrogen pressure in separate windows. Fig. 4 shows a typical multi-spectrum fit, including the observed spectra (black), calculated spectra (red), and the fit residual. The fit program divides the spectrum into micro-windows with a spectral width of $\sim$ 2 cm^{-1}; this makes the continuum baseline less critical in the fitting. In addition, the baseline in each microwindow was fitted to a quadratic polynomial to correct for any slant or curvature in the background continuum. The fitting was carried out for the lines in each microwindow at all the pressures at each temperature. The CH_4 molecules decompose at high temperatures ($\sim$ 800–1000 K) [44–46]. Therefore, the true methane pressure at higher temperature is less than the nominal pressure measured by the pressure gauge. To determine a more accurate methane partial pressure, a pressure calibration factor was calculated from a fit of the CH_4 number density. To determine a true methane number density for each spectrum, a single spectrum fit of methane line parameters including pressure broadening (γ_0) and pressure shifting (δ_0) was done for each pressure of H_2 at each temperature. The number density factor was adjusted for a number of selected lines while the line intensities were kept fixed at HITRAN 2012 [42] values. To evaluate the accuracy of these factors, a fitting error associated with each factor was also determined. A single factor was obtained by averaging the adjusted number density for the selected lines for every single spectrum at the given pressure. These adjusted number densities were used in the multi-spectrum fit. For example, the CH_4 pressure factor values calculated at 463 K for H_2 pressures of 50, 150, 240, 320 and 400 Torr were 0.92 (6E-4), 0.98 (6E-4), 0.98 (5E-3), 0.9 (2E-5), and 0.87 (5E-4), respectively, where the numbers inside the parentheses are the RMS values.

To examine the accuracy of the measured temperatures, a temperature fit was done from the retrieved CH_4 line strengths, for each single pressure. In this procedure, an initial fit was done using HITRAN 2012 [42] lines as the initial guess. Then the retrieved line absorptions were fitted using the reference line strengths by optimizing a factor for the temperature. Table 2 shows a comparison between the measured temperature and the temperature obtained by fitting spectra for all temperatures at 50 Torr of H_2.

As the initial guess, a multi-spectrum fit was carried out with initial line parameters taken from the HITRAN 2012 [42] with air as the broadening agent. Once an initial run of the multi-spectrum fit was done, the parameters with non-physical values or undetermined parameters were reset to the default value for the next iteration or set to zero.

Table 3
Double power law coefficients for temperature dependence of broadening parameters from Voigt profile.

Line	Voigt				
	C_1	n_1	C_2	n_2	RMSE
R(0)	-1.8208	-0.3468	2.8196	-0.1027	3.0×10^{-4}
R(1)	-1.1570	1.6414	2.1571	0.9940	7.30×10^{-4}
R(6) A_1–A_2	-4.4059	1.4323	5.4052	1.1971	5.60×10^{-4}
P(4) F_1–F_2	-3.9934	1.5341	4.9910	1.2098	7.95×10^{-4}
P(5) F_2–F_1	-3.6868	1.4637	4.6856	1.1592	4.46×10^{-4}
P(7) F_1–F_2	3.5556	1.1918	-2.5563	1.6483	3.37×10^{-4}

4. Results and discussion

4.1. Pressure-induced line broadening (γ_0)

Increasing hydrogen pressure leads to the broadening of spectral lines (see Fig. 3). These line broadenings depend on the temperature at which the spectrum is recorded. In the literature, temperature-dependence of the line broadening parameter is usually expressed in the single power law (SPL) form of

$$\frac{\gamma_0(T)}{\gamma_0(T_0)} = \left(\frac{T_0}{T}\right)^n, \tag{2}$$

in which γ_0 is the pressure-induced line broadening in cm^{-1}/atm units with T_0 = 296 K as the reference temperature, and n is the temperature-dependence coefficient. The SPL is derived under the assumptions that 1. the temperature range is small, 2. the intermolecular potential only contains one term; and 3. all collisions are on resonance [39]. In this study, a wider temperature range from 296 K to about 1100 K was used to investigate the broadening parameters of CH_4. Recent studies on the temperature-dependence of pressure-induced broadening show that in the case of wide temperature ranges the SPL is not sufficient to predict the temperature-dependence of line parameters [39]. Here, a double power law (DPL),

$$\gamma_0(T) = \gamma_0(T_0)[c_1\left(\frac{T_0}{T}\right)^{n_1} + c_2\left(\frac{T_0}{T}\right)^{n_2}], \tag{3}$$

was used to fit the temperature dependence of the pressure-induced broadening parameter (γ_0) in cm^{-1}/atm units, where c_1, n_1, c_2 and n_2 are constants to be determined. A non-linear least squares fit is conducted using the Nelder–Mead simplex method [47] to determine the c_1, n_1, c_2 and n_2 coefficients and root mean square error,

$$RMSE = \sqrt{\frac{\sum_{i=1}^{n}[Y_i(\text{data}) - Y_i(\text{model})]^2}{n}}, \tag{4}$$

was calculated. The n_1 and n_2, temperature-dependence coefficients, as well as c_1 and c_2 coefficients, for the line broadening parameter, were determined for both P and R branches in the ν_3 band of methane. Fig. 5 shows the pressure-induced broadening coefficients (γ_0) for the selected P(7) $F_1 - F_2$, P(5) $F_2 - F_1$, P(4) $F_1 - F_2$, R(0), R(1), and R(6) $A_1 - A_2$ lines, with associated DPL fit functions, in cm^{-1}/atm units versus temperature in kelvin. Coefficients of the DPL for the selected lines are presented in Table 3. Overall, the parameters obtained from the DPL, show a reasonable fit of temperature dependence of the γ_0 values. A complete table of DPL coefficients for the temperature-dependence of the broadening parameter is provided in supplementary Table S1. No error

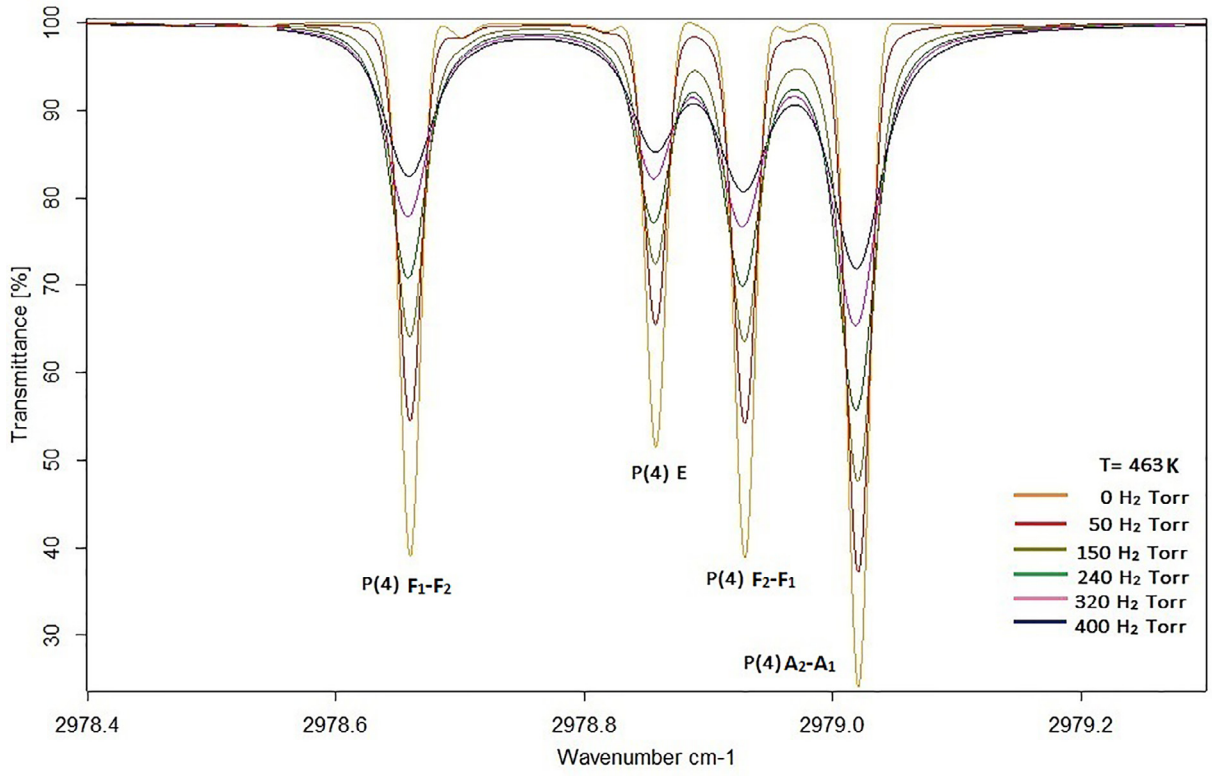

Fig. 3. Recorded spectra of P(4) line of the ν_3 band of CH_4 with assigned symmetries, with different pressures of H_2 and 0.5 Torr CH_4 pressure at 463 K.

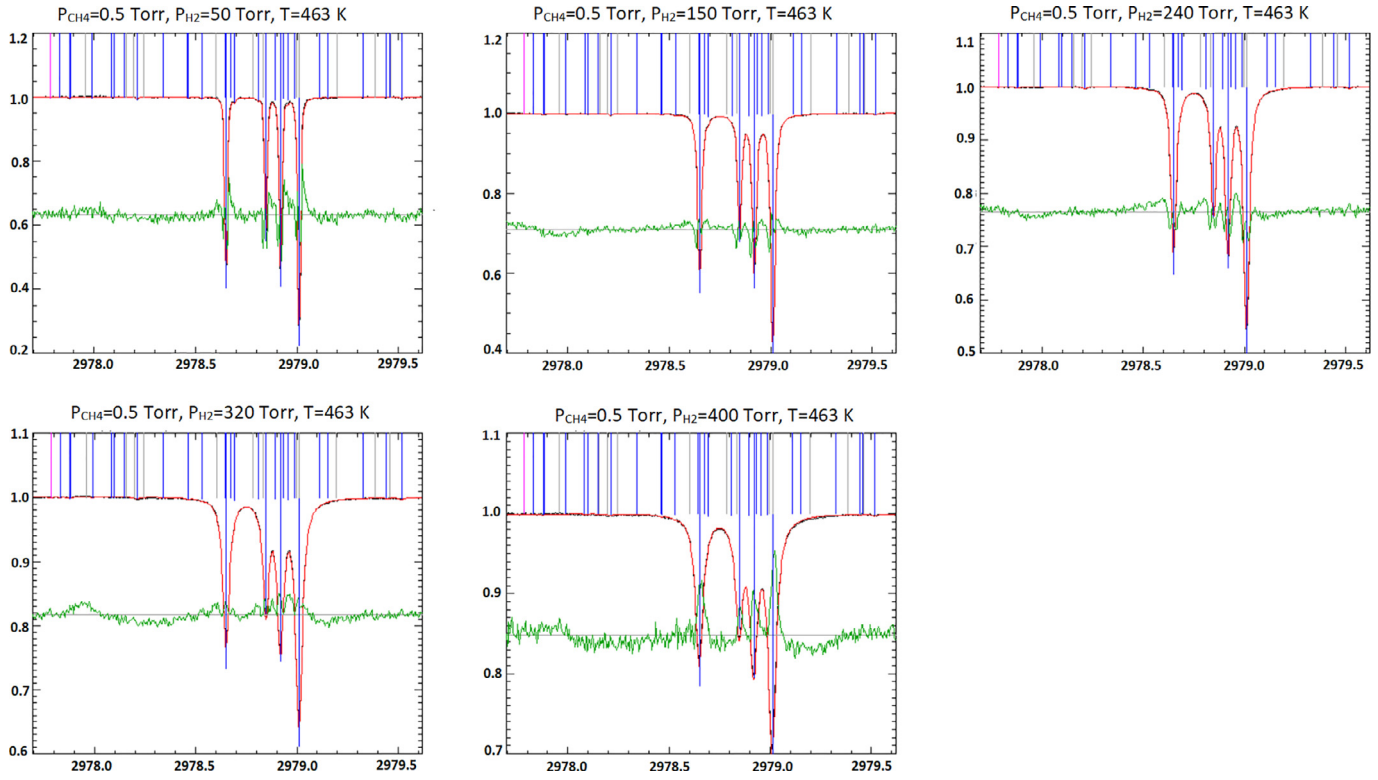

Fig. 4. A multi spectrum fit of measured lab spectra of P(4) line (black), the calculated spectrum (red) and the spectral residuals (green) magnified 10 times the vertical scale at 463 K. The vertical blue lines are the calculated CH_4 line positions.

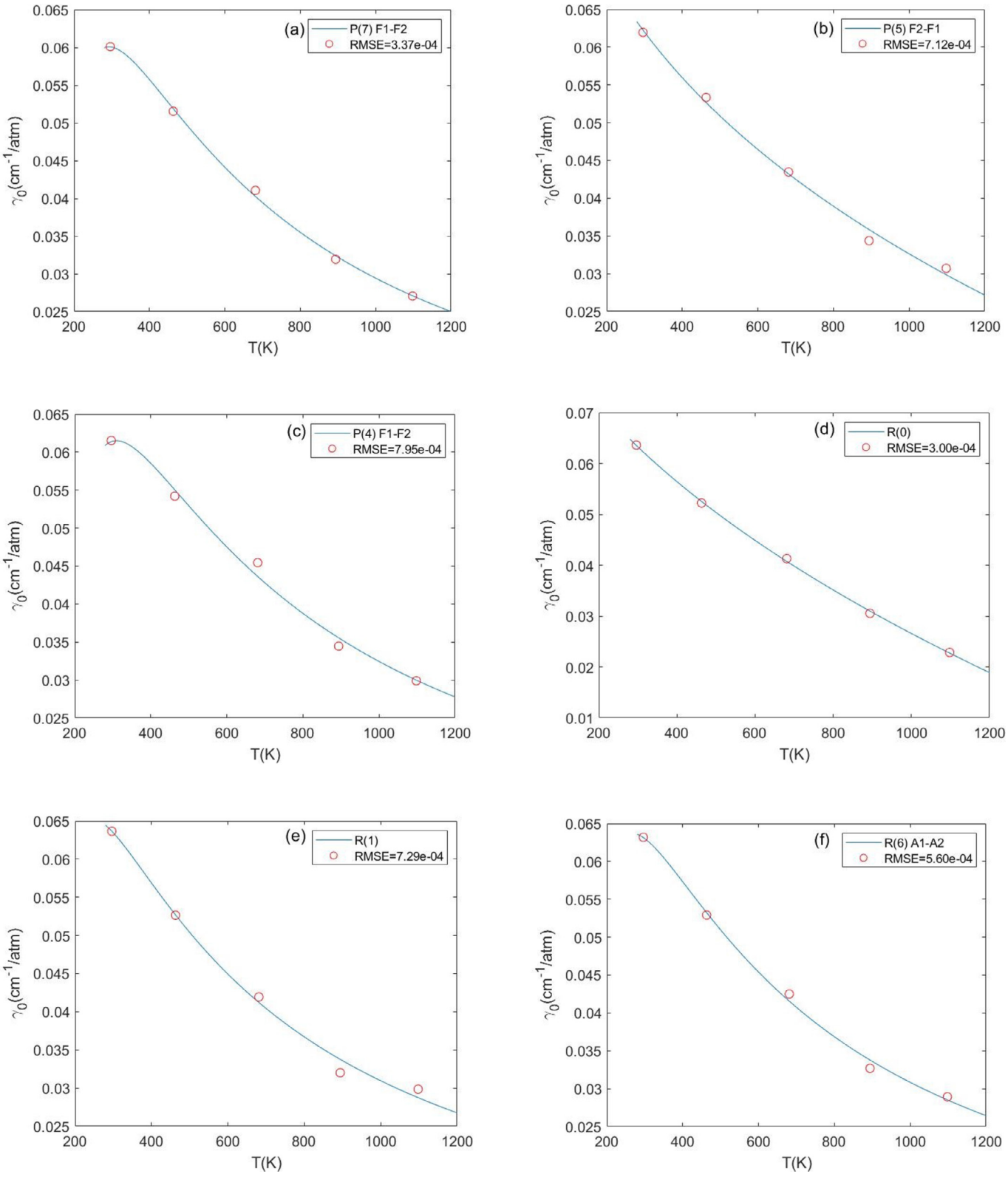

Fig. 5. Double power law fit to the broadening parameters for the selected (a) P(7) F_1–F_2, (b) P(5) F_2–F_1, (c) P(4) F_1–F_2, (d) R(0), (e) R(1), and (f) R(6) A_1–A_2 lines. Red circles show γ_0 values and blue solid lines are DPL fits.

estimates are available for these fitting parameters, because the fitting method used provided no parameter error estimates. The double power law is highly non-linear and other methods such as Levenberg–Marquardt, which provide errors, failed.

A SPL fit of γ_0 values was also done for the same methane lines presented in Fig. 5 and root mean square error values were obtained (Fig. 6). Comparison of temperature fitting of γ_0 shows improvement of fits from DPL over fits from SPL (see Figs. 5 and 6).

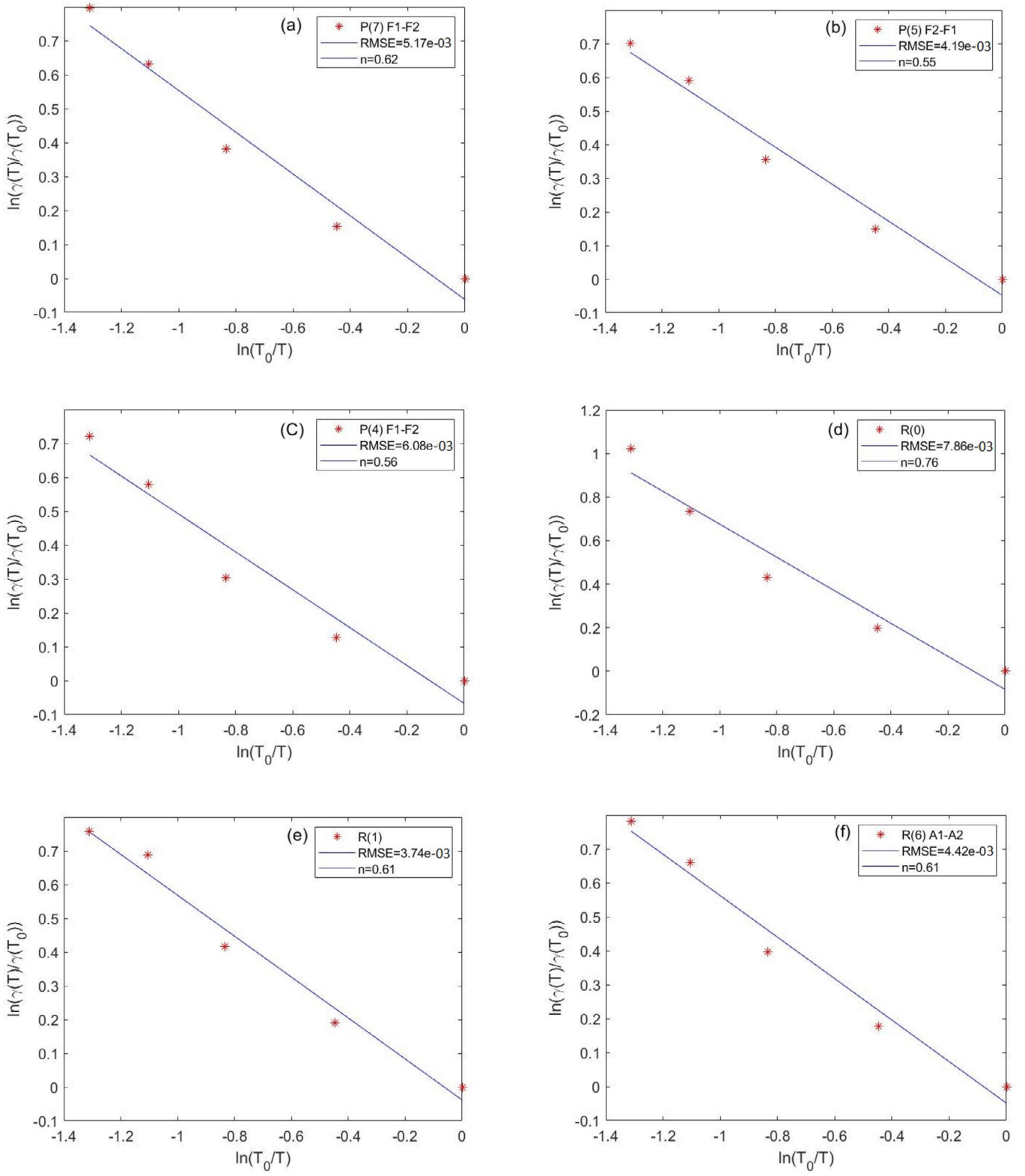

Fig. 6. Single power law fit to the broadening parameters for the selected (a) P(7) F_1–F_2, (b) P(5) F_2–F_1, (c) P(4) F_1–F_2, (d) R(0), (e) R(1), and (f) R(6) A_1–A_2 lines. The red asterisks show γ_0 values and the blue solid lines are SPL fits.

In addition, the rotational dependence of pressure-induced broadening coefficients is analyzed for the P and R branches of the ν_3 band. The γ_0 coefficients calculated using Voigt line profile are plotted versus rotational quantum number (J'') for 296 K, 463 K, 681 K, 894 K, and 1098 K, separately. Fig. 7 (a-e) shows J dependence of γ_0 coefficients for the aforementioned temperatures. To show the J dependence, a rotational quantum number index m is used, where $m = -J$ for the P branch, and $m = J + 1$ for the R branch. The J dependence of γ_0 for each A, E and F symmetry components within each J manifold is distinguished. The scat-

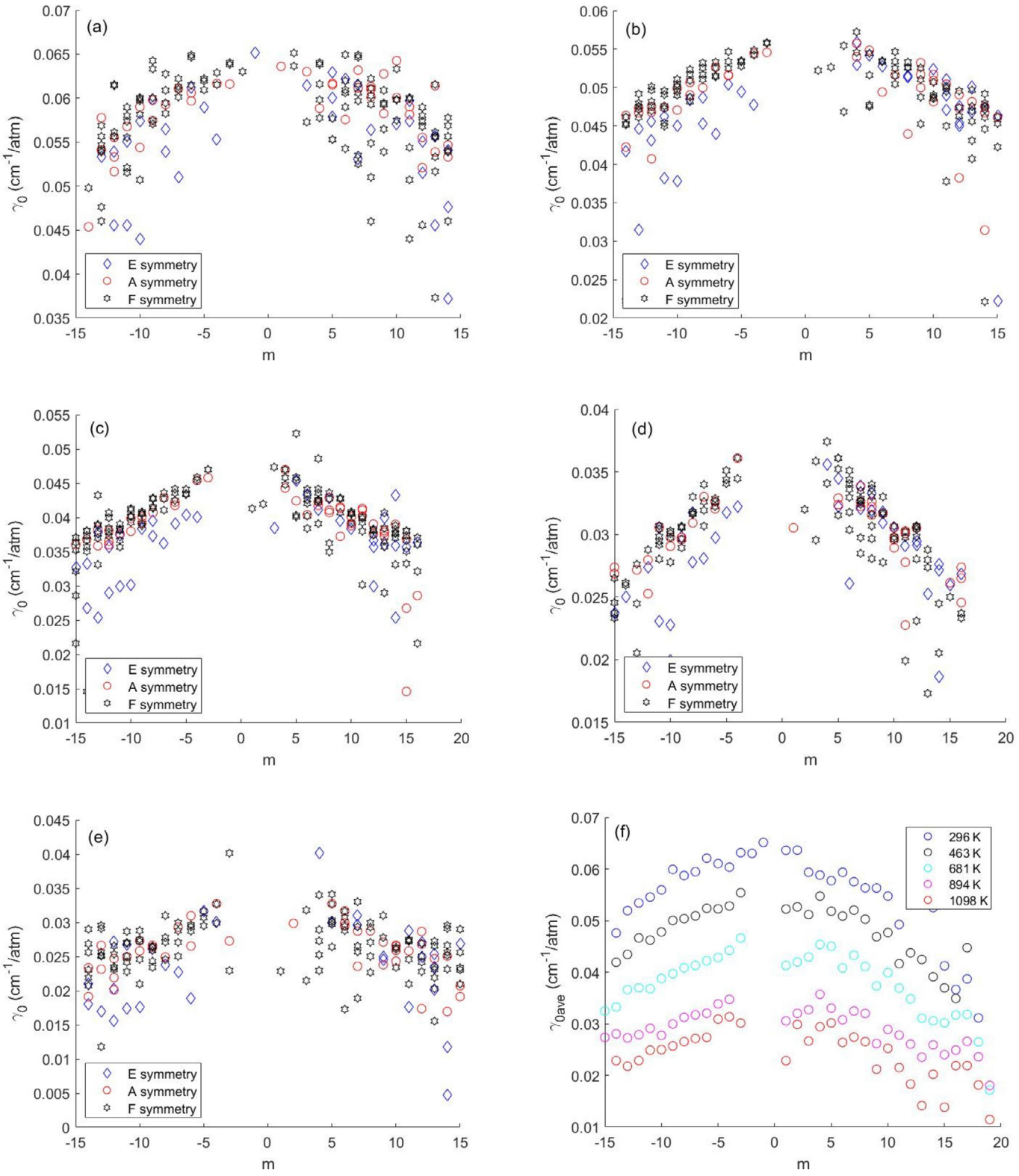

Fig. 7. Variation of pressure-induced broadening coefficients calculated using the Voigt profile with rotational quantum number index m. (m= - J for the P branch and m=J+1 for the R branch) at (a) 296 K, (b) 463 K, (c) 681 K, (d) 894 K, and (e) 1098 K. The broadening parameters are separated into A, E and F symmetries. The lines with E symmetry show weakest broadening. (f) is the J dependence of the γ_0 coefficients averaged over all symmetries.

ter among values at a single *J* value shows differences for transitions between different sub-levels. For instance, P(8) F_1–F_2 line has a different line broadening than the P(8) E line. Error bars are also included for γ_0 in Fig. 7. The fit errors are < 1% for γ_0 values with the exception of a few lines mostly at higher *J*s.

Overall, γ_0 shows a decreasing trend with increasing *m* for all temperatures. γ_0 values are distributed between (~ 0.065 – ~ 0.05) cm^{-1}/atm, (~ 0.055 – ~ 0.04) cm^{-1}/atm, (~ 0.047 – ~ 0.032) cm^{-1}/atm, (~ 0.037 – ~ 0.025) cm^{-1}/atm and (~ 0.034 – ~ 0.02) cm^{-1}/atm at 296 K, 463 K, 681 K, 894 K, and 1098 K tempera-

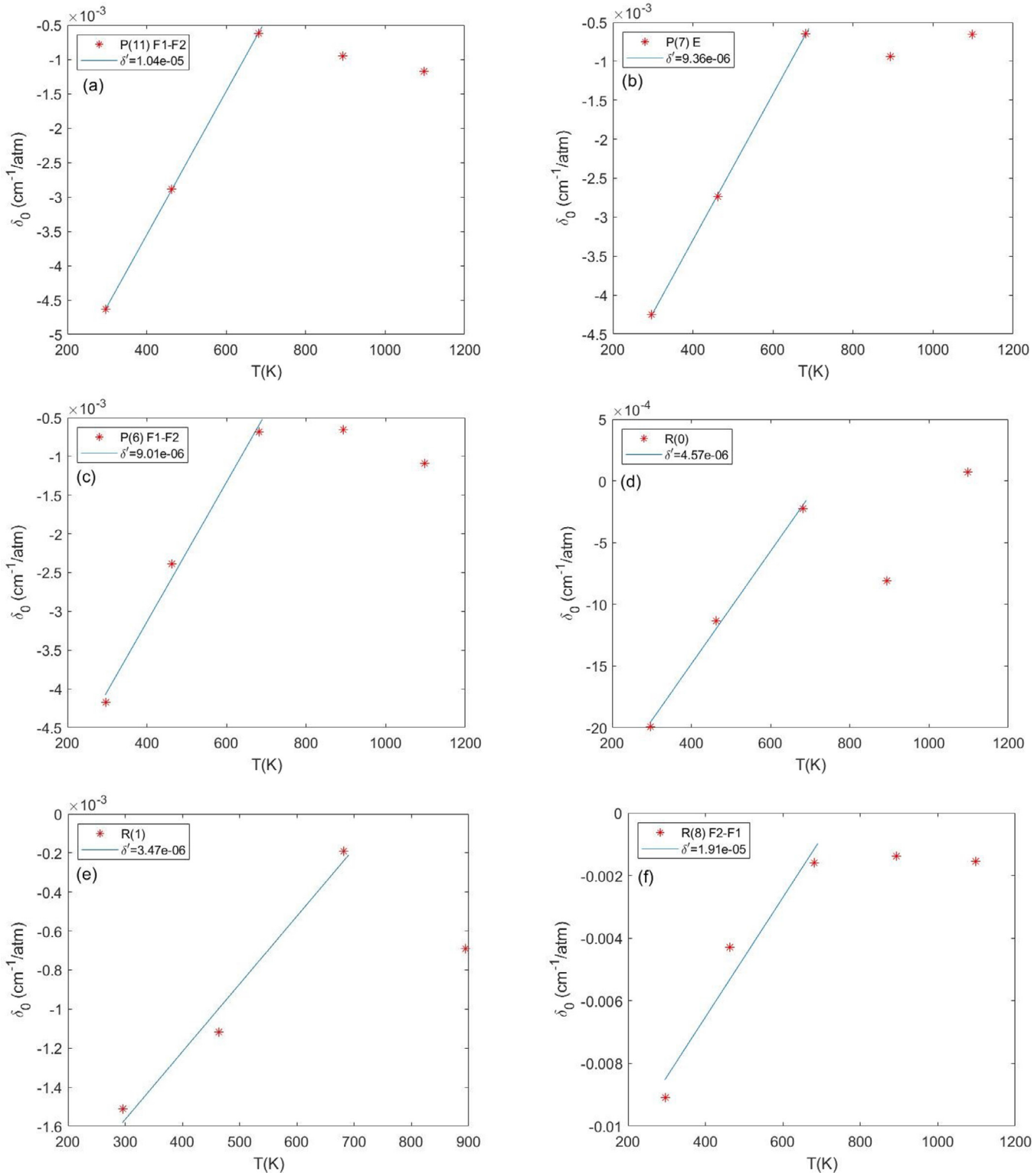

Fig. 8. Temperature-dependence of pressure shift (δ_0). The red asterisks show the line shift at each temperature and the solid blue line is the linear fit for the first three temperatures. The temperature dependent parameter (δ') for the selected (a) P(11) F_1–F_2, (b) P(7) E, (c) P(11) F_1–F_2, (d) R(0), (e) R(1), and (f) R(8) F_2–F_1, are 1.04×10^{-5} cm^{-1}/K, 9.36×10^{-6} cm^{-1}/K, 9.01×10^{-6} cm^{-1}/K, 4.57×10^{-6} cm^{-1}/K, 3.47×10^{-6} cm^{-1}/K, and 1.91×10^{-5} cm^{-1}/K, respectively. Note that only the first three temperatures were included in the fit.

tures, respectively. This shows a decrease of 20 to 30% for γ_0 with increasing J for temperatures up to 894 K and a 40% decrease in γ_0 with increasing J for 1098 K.

The symmetry dependence of γ_0 parameters show a weaker line broadening for E symmetry compared to the values corresponding to A and F symmetries, similar to previous observations [28,35]. Fig. 7 (f) also shows the J dependence of γ_0 values, averaged over each J manifold to remove the symmetry dependence, which also shows a decreasing trend with increasing m.

4.2. Pressure-induced line shift (δ_0)

Pressure-induced shifts are another consequence of collisions (H_2 in this work). Pressure shift parameters were determined by performing a multi-spectrum non-linear least squares fitting procedure, used in this study; data, including line position (σ), line intensity (S), pressure broadening (γ_0), shifting (δ_0) and their fitting errors are provided in supplementary tables S_2–S_6 for 296 K, 463 K, 681 K, 894 K, and 1098 K, respectively. In addition, temperature-dependence of pressure-induced shifts (δ_0) are studied. Conventionally, the temperature-dependence of δ_0 is expressed either in the power law form of

$$\delta_0(T) = \delta_0(T_0)\left(\frac{T_0}{T}\right)^q, \tag{5}$$

or in the linear form of

$$\delta_0(T) = \delta_0(T_0) + \delta'(T - T_0), \tag{6}$$

where $\delta_0(T)$ (in cm^{-1}/atm) is the pressure shift at temperature T, $\delta_0(T_0)$ (in cm^{-1}/atm) is the pressure shift at reference temperature $T_0 = 296$ K, q and δ' (in cm^{-1}/K) are the pressure shift coefficients for the power and linear forms, respectively.

The temperature-dependence of δ_0 obtained with the Voigt profile was studied. A linear increase of δ_0 values was observed for the lower temperatures 296 K, 463 K, and 681 K; however there is a deviation from a linear trend at 894 K and 1098 K. A linear form of δ_0 temperature-dependence was adopted but did not include data for 894 K and 1098 K. The reason for this deviation is not clear. A possible problem with the wavenumber calibration for the two highest temperatures could be the cause of these deviations. It is also worth mentioning that the linear form of temperature dependence only works for a limited temperature range. The deviation from the linear form at higher temperatures can be a result of the non-linearity of the temperature dependence of pressure shift parameters at higher temperature ranges. A linear fit of the first three temperatures was carried out to determine the temperature-dependence of pressure shift coefficients. Fig. 8 shows a linear fit for the temperature-dependence of δ_0 with a few selected lines, P(7) F_1–F_2, P(5) F_2–F_1, P(4) F_1–F_2, R(0), R(1), and R(6) A_1–A_2 with corresponding δ', which shows an increasing linear trend of δ_0 values with temperature. Table 4 lists a set of selected CH_4 lines with their corresponding temperature-dependence parameters (δ'). For the lines presented in Table 4, δ' coefficients range between 2.87×10^{-6} cm^{-1}/K and 8.66×10^{-5} cm^{-1}/K with an average value of 1.2×10^{-5} cm^{-1}/K.

Additionally, the J dependence of δ_0 parameters were analyzed. Symmetry dependence was also considered in the analysis. Rotational dependence of δ_0 values are shown in Fig. 9 (a-e).

The J dependence of the δ_0 parameter shows a different trend compared to γ_0. In the P branch, for the majority of lines, δ_0 values are less scattered and vary slowly with $|m|$. δ_0 values are distributed around ($\sim$ - 0.005, $\sim$ - 0.003) cm^{-1}/atm, ($\sim$ - 0.004, $\sim$ - 0.002) cm^{-1}/atm, ($\sim$ - 0.001, $\sim$ - 0.0005) cm^{-1}/atm, ($\sim$ - 0.0012, $\sim$ - 0.0005) cm^{-1}/atm, and ($\sim$ - 0.002, $\sim$ - 0.0005) cm^{-1}/atm for 296 K, 463 K, 681 K, 894 K, and 1098 K temperatures, respectively. Note that there are a few outliers from these limits especially at 1098 K. Overall, δ_0 values for the P branch with the exception of a few lines at 1098 K have negative values.

In the R branch, δ_0 are more scattered at each J and we observe significant variation in magnitude and sign of δ_0 values with increasing J (see Fig. 9). Overall, the pressure shift coefficients are distributed within the same limits as in the case of the P branch, but more outliers are observed compared to the P branch. Some of the δ_0 values in the R branch are positive (see Fig. 9) which means these lines, mainly those with F symmetry, are blue shifted. The spectral lines in the R branch are blended due to line mixing, es-

Table 4
Temperature-dependence parameters for pressure shift with their fitting error. Note that only the first three temperatures (296, 463, and 681 K) were included in the fit.

Line	δ'	error
P(13) E	8.05E-06	8.73E-06
P(13) A_1-A_2	8.98E-06	1.36E-05
P(12) F_1-F_2	3.64E-05	9.09E-05
P(12) A_1-A_2	1.86E-05	3.99E-05
P(12) F_1-F_2	7.76E-06	2.17E-05
P(12) E	8.22E-06	2.67E-05
P(12) F_2-F_1	1.10E-05	1.49E-05
P(12) F_1-F_2	1.02E-05	1.57E-05
P(12) A_2-A_1	5.53E-06	2.23E-05
P(11) E	7.79E-06	8.95E-06
P(11) F_1-F_2	2.22E-05	5.40E-05
P(11) F_2-F_1	7.23E-06	1.26E-05
P(11) E	8.75E-06	2.92E-05
P(11) F_1-F_2	1.04E-05	1.05E-05
P(11) A_1-A_2	8.60E-06	1.13E-05
P(11) F_1-F_2	9.08E-06	2.12E-05
P(11) F_2-F_1	5.12E-06	1.08E-05
P(10) E	7.32E-06	7.60E-06
P(10) F_2-F_1	1.63E-05	3.42E-05
P(10) A_2-A_1	7.52E-06	7.90E-06
P(10) F_2-F_1	8.83E-06	1.16E-05
P(10) F_1-F_2	1.12E-05	1.96E-05
P(10) A_1-A_2	1.01E-05	1.81E-05
P(10) F_1-F_2	1.15E-05	1.74E-05
P(9) F_2-F_1	2.23E-05	6.18E-05
P(9) E	1.06E-05	2.99E-05
P(9) F_1-F_2	8.86E-06	1.29E-05
P(9) F_2-F_1	1.05E-05	2.63E-05
P(8) E	6.60E-06	1.28E-05
P(8) F_2-F_1	1.64E-05	3.75E-05
P(8) F_1-F_2	8.40E-06	9.57E-06
P(8) F_2-F_1	7.18E-06	7.25E-06
P(8) A_2-A_1	9.51E-06	2.53E-05
P(7) E	9.36E-06	1.03E-05
P(7) F_1-F_2	1.32E-05	2.85E-05
P(7) A_1-A_2	8.95E-06	1.27E-05
P(7) F_1-F_2	8.80E-06	1.21E-05
P(6) A_2-A_1	5.44E-06	1.01E-05
P(6) F_1-F_2	1.89E-05	4.66E-05
P(6) A_1-A_2	1.27E-05	2.36E-05
P(6) F_1-F_2	9.01E-06	1.42E-05
P(6) E	1.04E-05	2.91E-05
P(5) F_2-F_1	5.40E-06	7.49E-06
P(5) E	1.05E-05	2.49E-05
P(5) F_1-F_2	1.31E-05	2.69E-05
P(5) F_2-F_1	9.84E-06	1.62E-05
P(4) F_1-F_2	7.03E-06	8.75E-06
P(4) E	9.28E-06	1.52E-05
P(3) F_1-F_2	6.02E-06	8.79E-06
P(3) F_2-F_1	1.41E-05	3.54E-05
R(0)	4.57E-06	6.22E-06
R(1)	3.47E-06	6.84E-06
R(2) E	2.87E-06	1.93E-05
R(3) A_1-A_2	3.26E-06	8.76E-06
R(3) F_2-F_1	7.75E-06	1.22E-05
R(4) A_2-A_1	4.67E-06	2.21E-05
R(5) F_1-F_2	1.02E-05	2.96E-05
R(5) F_2-F_1	4.67E-06	2.10E-05
R(6) A_1-A_2	9.93E-06	2.92E-05
R(6) F_1-F_2	1.25E-05	3.79E-05
R(7) F_1-F_2	1.01E-05	4.32E-05
R(8) F_2-F_1	1.91E-05	4.82E-05
R(9) A_2-A_1	2.01E-05	5.61E-05
R(10) A_2-A_1	6.76E-06	1.51E-05
R(11) A_1-A_2	3.92E-05	8.30E-05
R(12) F_1-F_2	8.66E-05	1.40E-04

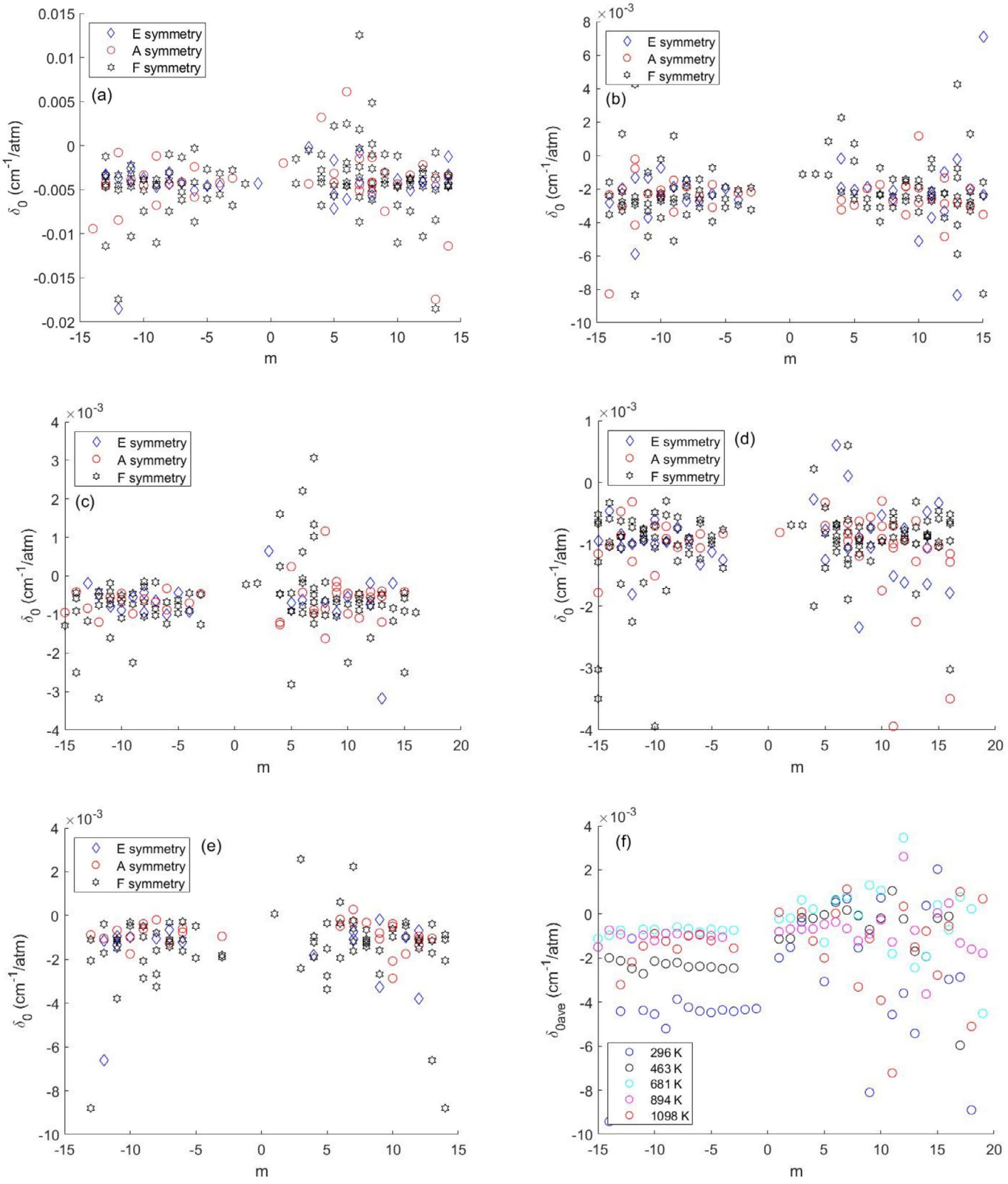

Fig. 9. Variation of pressure shift coefficients with rotational quantum number index m. (m= - J for P branch and m=J+1 for R branch) at (a) 296 K, (b) 463 K, (c) 681 K, (d) 894 K and (e) 1098 K. The shift parameters are separated into A, E and F symmetries. (f) is the J dependence of the δ_0 coefficients averaged over all symmetries.

pecially at higher pressures. Since the pressure-induced shifting is easily perturbed by the line mixing effect, the shifted lines could be affected by the lack of information on line mixing and should be further investigated.

A recent study by Gharib-Nezhad et al. [23] has reported the H_2 induced line broadening parameters in the P branch of the ν_3 band of CH_4 for the temperature range between 300–700 K. A comparison of the line broadening parameters was made between this study and the study of Gharib-Nezhad et al. [23] using six lines P(3) A_1-A_2, P(4) E, P(5) F_2-F_1, P(6) A_1-A_2, P(7) F_2-F_1, and P(9) F_2-F_1. The corresponding line broadening parameters were estimated using Eq. (4) from the study of Gharib-Nezhad et al. [23] at 463 K, and the temperature dependence coefficients were taken from the supplementary table provided by Gharib-Nezhad et al. [23]. Our line broadening parameters at 463 K for the selected lines are 0.054, 0.047, 0.053, 0.051, 0.051, and 0.051 cm^{-1}/atm, respectively. The broadening parameters for the same lines from the study of Gharib-Nezhad et al. [23] are 0.051, 0.047, 0.05, 0.05, 0.049, and 0.05 cm^{-1}/atm, respectively, which shows an average discrepancy of 3.3% between the values derived from the two studies.

5. Summary and conclusions

Spectra of CH_4 in the ν_3 band at five different 296 K, 463 K, 681 K, 894 K, and 1098 K temperatures were recorded using a high resolution (0.01 cm^{-1}) Fourier transform IR spectrometer. Five different pressures, 0 Torr, 50 Torr, 150 Torr, 240 Torr, 320 Torr and 400 Torr of H_2 were used as the broadening agent at each temperature. Transmission spectra of the ν_3 CH_4 band were obtained by correcting for the cell and CH_4 emission. The transmission spectra were calibrated using HITRAN 2012 [42]. Multi-spectrum least squares fits of CH_4 lines were carried out, at different H_2 pressures for each temperature.

Additionally, the temperature-dependence of the γ_0 and δ_0 parameters was also determined. Finally, the rotational transition dependence of pressure-induced broadening and shifting coefficients was studied. The results show a significant J dependence for the γ_0 coefficients. The γ_0 coefficients decrease about 20–30% for temperatures up to 894 K and about 40% for 1098 K, with increasing J quantum number. The δ_0 values are less scattered in the P branch compared to the R branch.

There are very few studies where the pressure-induced broadening and shift parameters at high temperatures are determined [23,41]. Our study provides a comprehensive set of pressure-induced broadening (γ_0) and shifting (δ_0) parameters, for both P and R branches, at high temperatures. Our data are intended to contribute to the spectroscopic analysis of H_2-dominated hot exoplanets and brown dwarfs.

Data availability

Complete tables including line positions (σ), line intensities (S) and measured pressure-induced broadening (γ_0), pressure shift (δ_0) coefficients are provided in tables S_1–S_6 separately for each temperature as supplementary data.

Declaration of Competing Interest

The authors declare that they have no known competing financial interests or personal relationships that could have appeared to influence the work reported in this paper.

CRediT authorship contribution statement

Mahdi Yousefi: Writing - original draft, Investigation, Data curation, Visualization. **Peter F Bernath:** Supervision, Conceptualization, Funding acquisition. **Mike Dulick:** Investigation. **Manfred Birk:** Software. **Georg Wagner:** Software.

Acknowledgments

This work is funded by the NASA Laboratory Astrophysics Program.

Supplementary material

Supplementary material associated with this article can be found, in the online version, at doi:10.1016/j.jqsrt.2021.107557

References

[1] Swain MR, Deroo P, Griffith CA, Tinetti G, Thatte A, Vasisht G. A ground-based near-infrared emission spectrum of the exoplanet HD 189733b. Nature 2010;463:637. doi:10.1038/nature08775.
[2] Guillot T, Gautier D. Giant planets. Treatise on Geophysics 2015;0:1–42.
[3] Guilluy G, Sozzetti A, Brogi M, Bonomo AS, Giacobbe P, Claudi R. Exoplanet atmospheres with GIANO–II. detection of molecular absorption in the day-side spectrum of HD 102195b. Astron Astrophys 2019;625:A107. doi:10.1051/0004-6361/201834615.
[4] Venot O, Agúndez M, Selsis F, Tessenyi M, Iro N. The atmospheric chemistry of the warm Neptune GJ 3470b: Influence of metallicity and temperature on the CH_4/CO ratio. Astron Astrophys 2014;562:A51. doi:10.1051/0004-6361/201322485.
[5] Moses JI, Line MR, Visscher C, Richardson MR, Nettelmann N, Fortney JJ. Compositional diversity in the atmospheres of hot Neptunes, with application to GJ436b. Astrophys J 2013;777:34. doi:10.1088/0004-637X/777/1/34.
[6] Beaulieu JP, Tinetti G, Kipping DM, Ribas I, Barber RJ, Cho JK. Methane in the atmosphere of the transiting hot Neptune GJ436b? Astrophys J 2011;731:16. doi:10.1088/0004-637x/731/1/16.
[7] Miller-Ricci E, Fortney JJ. The nature of the atmosphere of the transiting super-earth GJ 1214b. Astrophys J Lett 2010;716:L74. doi:10.1088/2041-8205/716/1/L74.
[8] Hand E. Super-earths give theorists a super headache. Nature 2011;480:302. doi:10.1038/480302a.
[9] Marley MS, Robinson TD. On the cool side: modeling the atmospheres of brown dwarfs and giant planets. Ann Rev Astro Astrophys 2015;53:279. doi:10.1146/annurev-astro-082214-122522.
[10] Owen JE. Atmospheric escape and the evolution of close-in exoplanets. Ann Rev Earth Planetary Sciences 2019;47:67. doi:10.1146/annurev-Earth-053018-060246.
[11] Orton GS, Fletcher LN, Moses JI, Mainzer AK, Hines D, Hammel HB. Mid-infrared spectroscopy of Uranus from the Spitzer infrared spectrometer: 1. determination of the mean temperature structure of the upper troposphere and stratosphere. Icarus 2014;243:494. doi:10.1016/j.icarus.2014.07.010.
[12] Lodders K. Exoplanet Chemistry. John Wiley & Sons, Ltd; 2010. doi:101002/9783527629763ch8. Ch 8: 157
[13] Visscher C, Moses JI. Quenching of carbon monoxide and methane in the atmospheres of cool brown dwarfs and hot Jupiters. Astrophys J 2011;738:72. doi:10.1088/0004-637X/738/1/72.
[14] Moses JI, Visscher C, Fortney JJ, Showman AP, Lewis NK, Griffith CA. Disequilibrium carbon, oxygen, and nitrogen chemistry in the atmospheres of HD 189733b and HD 209458. Astrophys J 2011;737:15. doi:10.1088/0004-637X/737/1/15.
[15] Line MR, Vasisht G, Chen P, Angerhausen D, Yung Y. Thermochemical and photochemical kinetics in cooler hydrogen-dominated extrasolar planets: a methane-poor GJ436b? Astrophys J 2011;738:32. doi:10.1088/0004-637X/738/1/32.
[16] Bernath P. Molecular opacities for exoplanets. Philos Trans Royal Soc A: Mathemat, Phys Eng Sciences 2014;372:20130087. doi:10.1088/0004-637X/738/1/32.
[17] Seager SV, Sasselov DD. Theoretical transmission spectra during extrasolar giant planet transits. Astrophys J 2000;537:916. doi:10.1086/309088.
[18] Yurchenko SN, Tennyson J, Bailey J, MDJ H, Tinetti G. Spectrum of hot methane in astronomical objects using a comprehensive computed linelist. Proc Nat Acad Sci 2014;111:9379. doi:10.1073/pnas.1324219111.
[19] Hill C, Yurchenko SN, Tennyson J. Temperature-dependent molecular absorption cross sections for exoplanets and other atmospheres. Icarus 2013;226:1673. doi:10.1016/j.icarus.2012.07.028.
[20] Freedman RS, Lustig-Yaeger J, Fortney JJ, Lupu RE, Marley MS, Lodders K. Gaseous mean opacities for giant planet and ultracool dwarf atmospheres over a range of metallicities and temperatures. The Astrophys J Supp 2014;214:25. doi:10.1088/0067-0049/214/2/25.
[21] Freedman RS, Marley MS, Lodders K. Line and mean opacities for ultracool dwarfs and extrasolar planets. The Astrophys J Supp 2008;174:504. doi:10.1086/52179.
[22] Varanasi P, Chudamani S. The temperature-dependence of lineshifts, linewidths and line intensities of methane at low temperatures. J Quant Spectrosc Radiat Transf 1990;43:1. doi:10.1016/0022-4073(90)90060-J.

[23] Gharib-Nezhad E, Heays AN, Bechtel HA, Lyons JR. H_2-induced pressure-induced broadening and pressure shift in the P-branch of the ν_3 band of CH_4 from 300 to 655 K. J Quant Spectrosc Radiat Transf 2019;239:106649. doi:10.1016/j.jqsrt.2019.106649.
[24] Fortney JJ. Modeling exoplanetary atmospheres: an overview (a chapter from astrophysics of exoplanetary atmospheres). Springer 2018;450:51. doi:10.1007/978-3-319-89701-1_2.
[25] Hedges C, Madhusudhan N. Effect of pressure broadening on molecular absorption cross sections in exoplanetary atmospheres. Month Notices of the Royal Astronom Society 2016;458:1427. doi:10.1093/mnras/stw278.
[26] Margolis JS. Hydrogen broadening and collision-induced line shifts of methane at 4200cm^{-1}. J Quant Spectrosc Radiat Transf 1993;49:71. doi:10.1016/0022-4073(93)90019-E.
[27] Margolis JS. Measurement of hydrogen-broadened methane lines in the ν_4 band at 296 and 200 K. J Quant Spectrosc Radiat Transf 1993;50:431. doi:10.1016/0022-4073(93)90073-Q.
[28] Smith MAH, Rinsland CP, Devi VM, Benner DC. temperature-dependence of broadening and shifts of methane lines in the ν_4 band. Spectrochemica Acta 1992;48:1257. doi:10.1016/0584-8539(92)80263-V.
[29] Devi VM, Benner DC, Smith MA, Rinsland CP. Measurements of air-, N_{2^-}, and O_{2^-} -broadened halfwidths and pressure-induced line shifts in the ν_3 band of $^{13}CH_4$. Appl optics 1991;30:287. doi:10.1364/AO.30.000287.
[30] Predoi-Cross A, Brawley-Tremblay M, Brown LR, Devi VM, Benner DC. Multispectrum analysis of $^{12}CH_4$ from 4100 to 4635cm^{-1}: II. air-broadening coefficients (widths and shifts). J Mol Spec 2006;236:201. doi:10.1016/j.jms.2006.01.013.
[31] Pine AS. Self-, N_2, O_2, H_2, Ar, and He broadening in the ν_3 band Q branch of CH_4. J Chem Phys 1992;97:773. doi:10.1063/1.463943.
[32] Anderson PW. Pressure-induced broadening in the microwave and infra-red regions. Physical Review 1949;76:647. doi:10.1103/PhysRev.76.647.
[33] Neshyba SP, Lynch R, Gamache R, Gabard T, Champion JP. Pressure-induced widths and shifts for the ν_3 band of methane. J Chem Phys 1994;101:9412. doi:10.1063/1.467972.
[34] Gabard T. Calculated line broadening parameters for methane perturbed by diatomic molecules. J Mol Spec 2013;291:61. doi:10.1016/j.jms.2013.05.011.
[35] Smith LN, Secrest D. Close-coupling and coupled state calculations of argon scattering from normal methane. J Chem Phys 1981;74:3882. doi:10.1063/1.441564.
[36] Tennyson J, Bernath PF, Campargue A, Császár AG, Daumont L, Gamache RR. Recommended isolated-line profile for representing high-resolution spectroscopic transitions (IUPAC technical report). Pure Appl Chem 2014;86:1931. doi:10.1515/pac-2014-0208.
[37] Loos J, Birk M, Wagner G. New multispectrum fitting software used at DLR for analysis of laboratory Fourier-transform molecular spectra. In 13th International HITRAN Conference 2014;206:296. doi:10.5281/zenodo.11156.
[38] Wilzewski JS, Birk M, Loos J, Wagner G. Temperature-dependence laws of absorption lineshape parameters of the $CO_2\nu_3$ band. J Quant Spectrosc Radiat Transf 2018;206:296. doi:10.1016/j.jqsrt.2017.11.021.
[39] Gamache RR, Vispoel B. On the temperature-dependence of half-widths and line shifts for molecular transitions in the microwave and infrared regions. J Quant Spectrosc Radiat Transf 2018;217:440. doi:10.1016/j.jqsrt.2018.05.019.
[40] Delahaye T, Ghysels M, Hodges JT, Sung K, Armante R, Tran H. Measurement and modeling of air-broadened methane absorption in the MERLIN spectral region at low temperatures. J Geophys Res: Atmospheres 2019;124:3556. doi:10.1029/2018JD028917.
[41] Sung K, Devi VM, Benner DC, Drouin BJ, Crawford TJ, Mantz AW, Smith MA. H_2-pressure broadening and frequency shifts of methane in the $\nu_2 + \nu_3$ band measured in the temperature range between 80 and 370 K. J Quant Spectrosc Radiat Transf 2020;256:107264. doi:10.1016/j.jqsrt.2020.107264.
[42] Rothman LS, Gordon IE, Babikov Y, Barbe A, Benner DC, Bernath PF, et al. The HITRAN2012 molecular spectroscopic database. J Quant Spectrosc Radiat Transf 2013;130:4. 10.1016/j.J Quant Spectrosc Radiat Transf.2013.07.002
[43] Bernath PF. Spectra of atoms and molecules. 4rd edition. (Oxford University Press); 2020.
[44] Willacy K, Klahr HH, Millar TJ, Henning T. Gas and grain chemistry in a protoplanetary disk. Astronom and Astrophys 1998;338:995.
[45] Hargreaves RJ, Bernath PF, Bailey J, Dulick M. Empirical line lists and absorption cross sections for methane at high temperatures. The Astrophys J 2015;813:12. doi:10.1088/0004-637x/813/1/12.
[46] Chen CJ, Back MH, Back RA. Mechanism of the thermal decomposition of methane. The Astrophys J 1976;32:1. doi:10.1021/bk-1976-0032.ch001.
[47] Lagarias JC, Reeds JA, Wright MH, Wright PE. Convergence properties of the Nelder-Mead simplex method in low dimensions. SIAM J on optimization 1998;9:112. doi:10.1137/S1052623496303470.